Journal of Materials Chemistry A

Accepted Manuscript

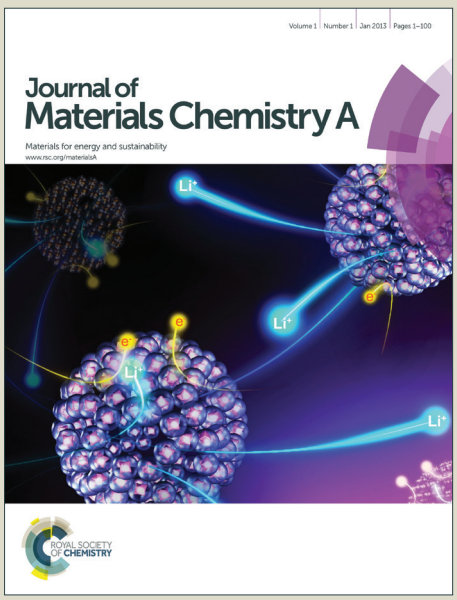

ROYAL SOCIETY OF CHEMISTRY

www.rsc.org/materialsA

Journal Name

ARTICLE

Coal derived porous carbon fibers with tunable internal channel for flexible electrodes and organic matter absorption

Received 00th January 20xx,
Accepted 00th January 20xx

DOI: 10.1039/x0xx00000x

www.rsc.org/

Mingxi Guo, Jixi Guo, Dianzeng Jia,* Hongyang Zhao, Zhipeng Sun, Xianli Song, Yinhua, Li

Coal-derived porous carbon fibers (CPCFs) were prepared by single-nozzle electrospinning the aqueous solution of acid treated coal and polyvinyl alcohol followed by thermal treatment in an inert atmosphere. The production yield of CPCFs was about 92% from coal. The structural, textural, and surface properties of CPCFs were investigated by means of spectroscopic, microscopy, and Brunauer-Emmet-Teller (BET) techniques. The results showed that the flexible CPCFs had abundant pore structure and large specific surface area. The electrochemical performance of supercapacitor electrodes with this fiber mats was studied. This binder free electrode showed a capacitance of 170 F g^{-1} at the current density of 1 A g^{-1} in 6 M aqueous KOH electrolyte. The electrode also showed stable cycling performance without any decrease in the specific capacitance after 20,000 charge/discharge cycles at the current density of 2 A g^{-1}. Besides, the CPCFs was superhydrophobic, and showed outstanding performance in oil-absorption and good circulation for remove dyes from water. These outstanding properties potentially make the flexibly CPCFs a promising candidate for energy storage and environmental protection.

Introduction

Carbon materials are ubiquitous in various technological and energy-related applications, including separation, catalysis, and energy storage/conversion because of their unique physicochemical properties.[1-6] Among various carbon materials, porous carbon materials have attracted more attention because of their high specific surface area and abundant pore structure.[7-12] At present, the research of porous carbon materials focuses on activated carbon, mesoporous carbons,[13,14] carbon foam,[15,16] and carbon fibers.[17-20] Porous carbon fibers as kind of new porous carbon materials, which retains a one-dimensional structure, has a high specific surface area, more active sites and abundant inner spaces, and is considered to have a great potential application in energy and environment.[21] According to the reports in the literature, electrospinning with sacrificial templates is a facile way to prepare porous carbon nanofibers.[22-28] The most widely used sacrificial templates are metal oxide nanoparticles and low-carbon-yield polymers.[22-26] Although metal oxide nanoparticle sacrificial templates are tunable in morphology, the tedious washing procedure hindered their practical application.[27] Low-carbon-yield polymers are the other kind of sacrificial templates for fabricating mesoporous carbon nanofibers. It was reported by Kim et al. that hollow porous carbon nanofibers can be obtained by pyrolysis of the electrospun products of polyacrylonitrile/poly(methyl methacrylate) mixture.[28] This method is easy to scale up because the hollow nanofibers can be obtained without co-axial electrospinning.

Biomass based carbon nanofibers are drawing much of attention these years.[29,30] One of the most significant advantages of biomass-derived carbon fiber is their abundant source and low cost. Coal is a traditional energy resource for electricity and heat production. They can be also fabricated into new carbon material such as activated carbon,[31,32] carbon nanotube,[33] and graphene quantum dots.[34] Recently, our group developed a method to prepare carbon fibers from coal.[35] In that study we found that the carbon-yield of acid treated coal was around 50%. However, it is hardly to widely use because the acid treated coal need to be dissolved in polar organic solvents, which is not economic.

Herein, we report a new method of preparation of coal-carbon fibers. Firstly, the coal was treated by the mixture of concentrated sulfuric acid and nitric acid, and the acid treatment coal can be dissolved in alkaline aqueous solution. And then the coal-derived porous carbon fibers ($CPCF_S$) was prepared by single-nozzle electrospinning using polyvinyl alcohol (PVA)/coal aqueous solution as precursor followed by carbonization. Coal contributed to the carbon component, and PVA acted as a sacrificial template for creating pores in the fibers. The morphology, pore structure, and chemical structure analysis were detailed investigated by electron microscopy,

Key laboratory of material and technology for clean energy, ministry of education; Key laboratory of advanced functional materials, autonomous region; Institute of Applied Chemistry, Xinjiang University, Urumqi 830046, Xinjiang, P. R. China. Tel.: +86-991-8583083; Fax: +86-991-8588883; E-mail address: jdz0991@gmail.com

Electronic Supplementary Information (ESI) available: Photograph of CPCFs as flexible material; XRD patterns of raw coal, acid treated coal and CPCFs; electrochemical performance of CPCFs measured in 6 M KOH electrolyte in two-electrode system; the water contact angle of CPCFs. See DOI: 10.1039/x0xx00000x

and Brunauer-Emmet-Teller (BET) techniques. We found that the coal-derived porous carbon nanofibers showed excellent cycle stability when used as a flexible binder-free supercapacitor electrode, and showed outstanding performance in oil-absorption, and good circulation for remove dyes from model wastewater of sample.

Experimental

Materials

Coal was obtained from Heishan, Xinjiang, China. An industrial analysis of the raw coal components is shown in Table 1. PVA, H_2SO_4 (98%), HNO_3 (63%), sodium dodecyl benzene sulfonate (SDBS) and methyl blue (MB) were analytical grade and were used without further purification. Cottonseed oil was purchased commercially and used without further purification. Distilled water was used throughout the experiments.

Spinning dope preparation

The fine raw coal powders was treated by mixed acid (V_{HNO3}/V_{H2SO4} = 1:3) as previously reported by our group.[35] The acid treated coal was added into distilled water followed by ultrasonication and then neutralized with SDBS to give 4 wt% and 8 wt%. A certain amount of PVA was added into black solution with stirring at 80 °C for 2 h. The solutions for electrospinning were prepared with different PVA/coal mass ratios of 1/2 (0.4 g/0.8 g), 1/1 (0.8 g/0.8 g) and 2/1 (0.8 g/0.4 g).

Electrospinning

The electrospinning setup purchased from Beijing Ucalery Technology Development Co., Ltd. A nozzle with an inner diameter of 0.8 mm served as the positive electrode. The nozzle and collector were place 20 cm apart and a potential of 20 kV was applied between them. Fibers were collected on an aluminum foil, which severed as the negative electrode.

Carbonization of fibers

The coal based porous carbon fibers were obtained by a two-step heat-treatment process including stabilization in air atmosphere at 200 °C for 3 h with a heating rate of 1 °C min^{-1}, and then carbonization in N_2 atmosphere at 800 °C for 2 h with a heating rate of 5 °C min^{-1}. Fig. 1 shows schematic illustration of the fabrication of CPCFs.

Table 1 Component analysis of raw coal

Proximate analysis (wt%)			Ultimate analysis (wt%)			
M_{ad}	A_d	V_{daf}	C_d	H_d	O_d	N_d
3.08	1.09	34.01	81.27	4.54	12.02	0.76

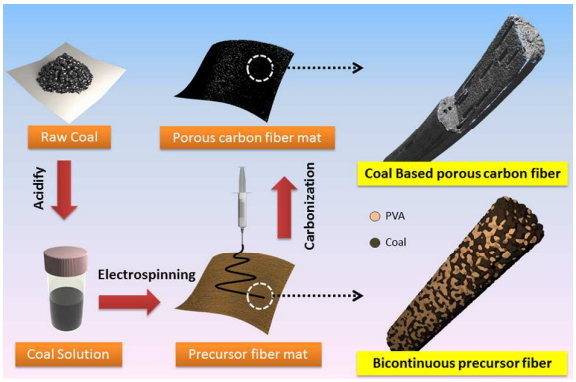

Fig. 1 Schematic illustration of the fabrication of CPCFs.

Structural characterization

Thermogravimetric analysis (TGA) was monitored using a NETZSCH STA449F3-QMS403C instrument with a heating rate of 10 °C/min from room temperature to 850 °C under a flow of nitrogen. Field emission scanning electron microscopy (FESEM) images were obtained by using a Hitachi S-4800 microscope at an accelerating voltage of 5 kV. The morphology of the samples was examined by transmission electron microscopy (TEM; H-600; 100 kV). High resolution transmission electron microscope (HRTEM) images of the products were obtained on a JEOL JEM-2010F electron microscope with an accelerating voltage of 200 kV. The infrared spectroscopy study was carried out using a Bruker VERTEX 70 Fourier transform infrared (FT-IR) spectrometer in a range of wavenumbers from 400 to 4000 cm^{-1}. Raman spectroscopy was performed on a Bruker SENTERRA dispersive Raman microscope using a 532 nm laser. Powder X-ray diffraction (XRD) measurements were conducted on a Bruker D8 Advance Diffraction diffractometer in the 2θ range from 5° to 80°, with Cu Kα radiation (λ = 0.15405 nm) at 40 kV and 40 mA. The Brunauer-Emment-Teller (BET) and Barret-Joyner-Halender (BJH) results were measured on a Micromeritics ASAP 2020 surface area and porosity analyzer. The solubility of the coal was measured by dissolving an excess amount of coal in aqueous solution, followed by subtracting the residual mass from the initial mass. Contact-angles measurements were performed with Powereach JC2000C at ambient temperature. UV-visible absorption spectra were studied using a Hitachi U-3010 spectrometer.

Electrochemical characterization

The electrochemical experiments were carried out using three-electrode system and two-electrode system at ambient condition. The produced fiber mats were directly used as a flexible binder-free working electrodes (Fig. S1). The size of electrode was 1 cm × 1 cm. The electrochemical tests were performed in a three-electrode cell, in which platinum foil and saturated calomel electrode (SCE) were used as counter and reference electrodes, respectively. The two-electrode system was measured by assembling a symmetrical capacitor with 6 M KOH. Cyclic voltammetry (CV) and galvanostatic charge-

discharge measurements were carried out on an electrochemical workstation (CHI760E, Shanghai Chenhua Device Company, China). The cycling performance of the electrode was evaluated on a Land battery measurement system (CT2001A, Wuhan LAND Electronics Co., Ltd).

Oil/water separate

The CPCFs (1 mg) was immersed into cottonseed oil (1 g) on the surface of excess water for seconds. Direct combustion in air was applied in order to remove the oil in the fiber mat; The mass of fiber mat was weighed after each cycle.

Dye removal

The model wastewater solution of 10 mg L^{-1} of MB was prepared. Put 1 mg CPCFs into 5 ml MB aqueous solution and kept for 12 h. The dye concentration was determined by UV-Vis spectrophotometer. The percent removal of MB was calculated by Eq. (1): Removal (%) = $(1-C/C_0) \times 100\%$. Where C_0 (mg L^{-1}) is the initial concentration of dye solution, C (mg L^{-1}) is the concentration of dye solution at contact time.

Results and discussion

Structure characterization

According to the coal structure model, the aromatic units are connected by aliphatic chains.[36,37] After treating with mixture of concentrate sulfuric acid and nitric acid, the weak aliphatic bonds between the macromolecule units were partially broken down leading to the disintergration of coal structure. Simultaneously, some oxygen-containing functional groups such as carboxyl, nitro, hydroxyl or sulfonic groups are formed, making the acid treatment coal soluble in both alkaline solutions and some polar organic solvents. As shown in Fig. 2, acid treated coal, raw coal/SDBS, and acid treated coal/SDBS were dispersed in H_2O. After 3 days, only acid treated coal/SDBS remained a homogeneous dispersion. SDBS was used as was used as neutralizing agent and dispersing agent. The solubility of acid treated coal is more than 8 wt% in aqueous solution

The surface functional groups of the raw coal and acid treated coal were investigated by FT-IR spectroscopy. After acid treating coal, a variety of surface functional groups were introduced into surface, as can be seen from Fig. 3. These functional groups centered at 3446, 2768, 1720, 1535 and 1114 cm^{-1} could be ascribed to -OH, $-NH_2$, -C=O, $-NO_2$ and $-SO_3H$, respectively. This results indicated that oxidation of the raw coal treated by a mixture of sulfuric acid and nitric acid, resulting in the formation of hydrophilic groups.

XRD profiles of the raw coal, acid treated coal, and CPCFs are shown in Fig. S2. It shows that raw coal and acid treated coal exhibit the wide (002) and (100) peaks of graphitic carbon around 24° and 43°. The reflection peaks of raw coal and acid treated coal are nearly identical, except that the peaks around

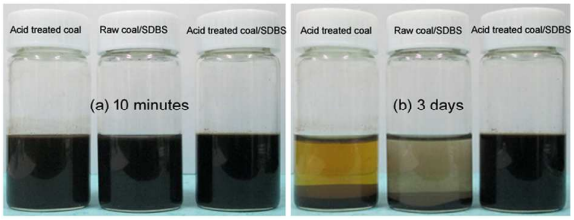

Fig. 2 Optical photographs of acid treated coal, raw coal/SDBS, and acid treated coal/SDBS dispersed in water. (a) Samples dispersed in water for 10 minutes. (b) After standing for 3 days, only acid treated coal/SDBS dispersion remained homogeneous in water.

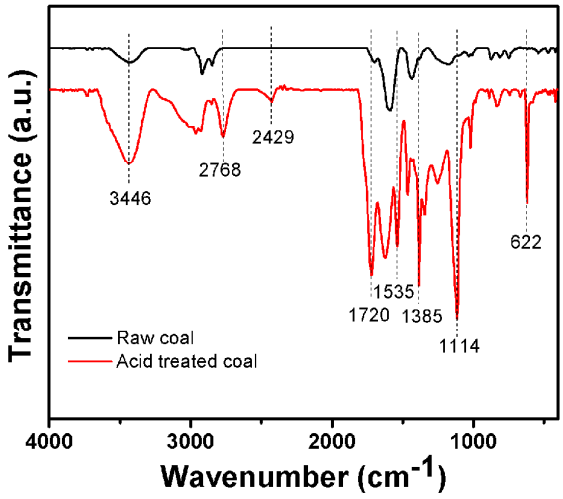

Fig. 3 FT-IR spectra of raw coal and acid treated coal.

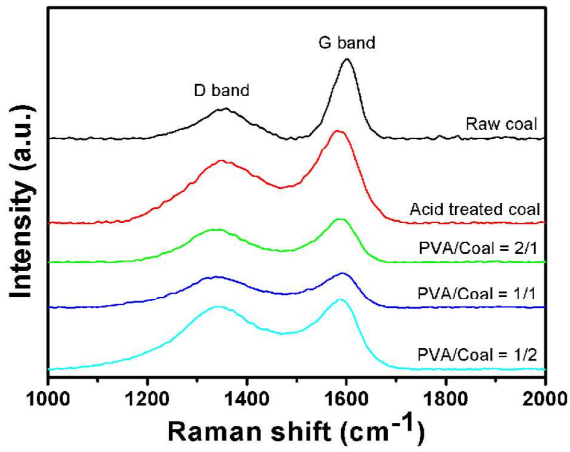

Fig. 4 Raman spectra of raw coal, acid treated coal and CBPCFs.

29°, 30°, 32° and 40° have disappeared for the acid treated sample, which can be attributed to the elimination of mineral components during acid treatment. Comparing with raw coal and acid treated coal, the peaks of the CPCFs are shifted to a relatively high angle, which can be attributed to the decreased interlayer spacing d_{002} during carbonization.

Raman spectroscopy was adopted to study the graphitization degree of the raw coal, acid treated coal and CPCFs (Fig. 4). The peaks around 1340 and 1600 cm^{-1} are

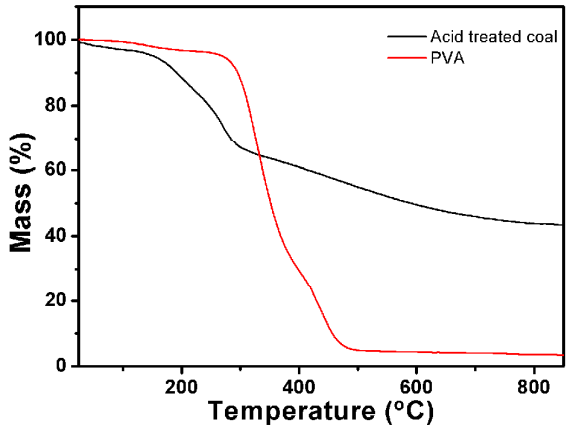

Fig. 5 TGA curves of acid treated coal and PVA.

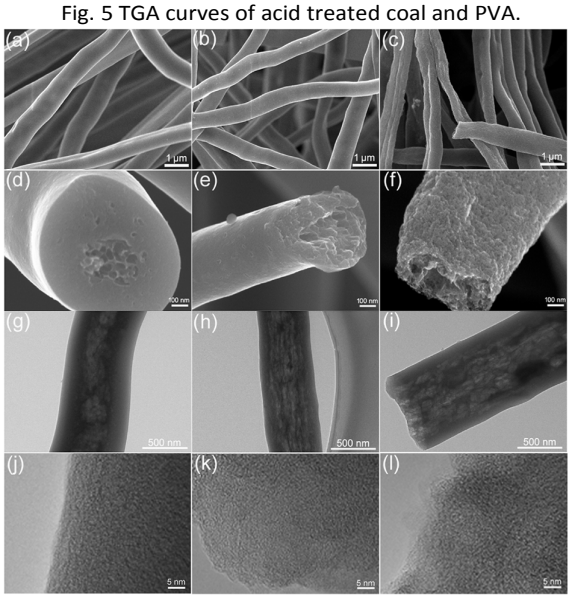

Fig. 6 (a, b, c) FESEM image of CPCFs at low magnification. PVA/Coal = a) 2/1, b) 1/1, and c) 1/2. (d, e, f) Magnified FESEM image of CPCFs. PVA/Coal = d) 2/1, e) 1/1, and f) 1/2. (g, h, i) TEM image of CPCFs. PVA/Coal = g) 2/1, h) 1/1, and i) 1/2. (j, k, l) HRTEM image of CPCFs. PVA/Coal = j) 2/1, k) 1/1, and l) 1/2.

identified as the D band and G band, respectively. The intensity ratio of D band to G band, *i.e.* $R_{(ID/IG)}$, were 0.38 and 0.72 for raw coal and acid treated coal. It can be inferred that some of the lamellar structures of graphene layers in the raw coal were destroyed during the acid treatment. The R values of CPCFs were similar to that of acid treated coal. The R value were 0.75, 0.90, and 0.88 for PVA/Coal = 2/1, PVA/Coal = 1/1 and PVA/Coal = 1/2, respectively, indicating the amorphous carbon structure was retained even after carbonization at 800 °C.

From thermogravimetric analyses of PVA and acid treated coal (Fig. 5). We know that PVA will lose more than 96% of its initial weight and the acid treated coal will lose 56% of the weight under nitrogen atmosphere at 800 °C. Finally, the production yield of CPCFs is about 92% from coal. Therefore, the acid treated coal was the primary carbon source of porous carbon fibers, PVA was used to help the formation of the fibers during electrospinning as well as the template for creating pores and channel.

As shown in low magnification FESEM (Fig. 6a,b,c), the carbon fibers exhibit long fibrous morphology, and homogeneous diameter distributions in the range of 500-800 nm. However, with the decreasing the fraction of PVA, the shape of fibers become irregular. This phenomenon may be caused by PVA as a binder to reduce. The magnified FESEM image of fibers (Fig. 6d,e,f) shows some channel in a single coal-based carbon fibers, and the outer surface roughness of the fibers increased with the coal increased. In addition, TEM image of samples (Fig. 6g,h,i) indicate that the long but discontinuous channel are well-developed along the fiber length. The PVA phase disappears without carbon residue and the coal phase is easily transformed into carbon during thermal treatment, many channels are created within a single carbon fibers as a result. It is therefore concluded that the patterns of pore structures as well as the porosity of the carbon fibers can be well controlled by tuning the different ratio of PVA and coal content. From HRTEM image (Fig. 6j,k,l), we found that the carbon in these CPCFs was amorphous.

The SSA and the pore size distribution of obtained samples were studied using Nitrogen adsorption/desorption isotherms at 77 K. As shown in Fig. 7a, all samples followed the hysteresis of type IV isotherms. The uptake at low pressure (< 0.2 P/P_0) indicates the presence of microporosity, and the adsorption at high pressure (> 0.8 P/P_0) indicates the presence of mesoporosity. This mesoporosity originates from the mesopores on outer surface and the hollow cores of the fibers. The porosity parameters for all samples are summarized in Table 2. The BET specific surface area and the volume of micropore increase with the content of coal. But the total pore

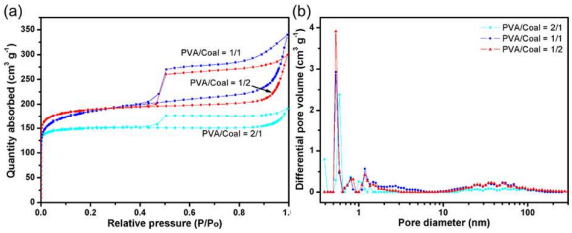

Fig. 7 (a) Nitrogen adsorption/desorption isotherms at 77 K and (b) pore size distribution curves of for three porous carbon fiber samples.

Table 2. Suface parameters of the porous carbon fibers

PVA/Coal mass ratios	S_{BET} [a] ($m^2\ g^{-1}$)	V_{total} [b] ($cm^3\ g^{-1}$)	V_{meso} [c] ($cm^3\ g^{-1}$)	V_{micro} [d] ($cm^3\ g^{-1}$)	D_{ap} [e] (nm)
2/1	604	0.295	0.067	0.211	1.96
1/1	691	0.526	0.27	0.226	3.04
1/2	728	0.463	0.185	0.249	2.51

[a] S_{BET}: specific surface area calculated by the BET method. [b] V_{total}: total pore volume at P/P_o = 0.99. [c] V_{meso}: volume of mesopore (1.7-300 nm) calculated using the BJH method based on the K elvin equation. [d] V_{micro}: micropore volume calculated using the Horvath-Kawazoe (HK) method. [e] D_{ap}: average pore size ($D_{ap} = 4V_t/S_{BET}$).

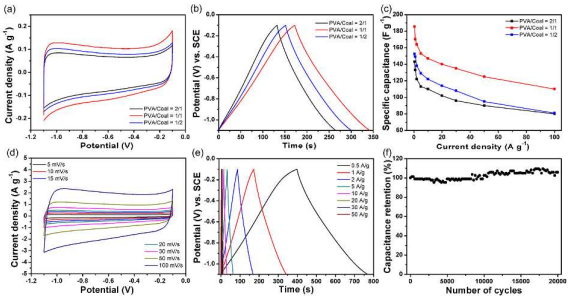

Fig. 8 (a) CV curves of three samples at the scanning rate of 5 mV/s. (b) Galvanostatic charge-discharge of three samples at specific capacitance of 1 A g^{-1}. (c) Specific capacitance of three samples at different specific currents. (d) CV curves of PVA/Coal = 1/1 at different scanning rates. (e) Galvanostatic charge-discharge curves of PVA/Coal = 1/1 at different specific currents. (f) The cycle lifetime of PVA/Coal = 1/1 at 2 A g^{-1}.

volume, the volume of mesopore (1.7-300 nm), and average pore size of PVA/Coal = 1/1 are larger than other samples (Fig. 7b and Table 2). This may be due to the complex gas evolution involved of degradation of PVA and carbonization of coal during thermal treatment is closely relates to pore formation. Therefore, we were able to tailor the surface area and pore size of the nanofibers simply by changing the mass ratio of PVA and coal because the PVA decomposes and the coal pyrolysis in a single nanofiber played a key role in mesopore formation during thermal treatment.

Electrochemical characterization

Fig. 8 exhibits the electrochemical performance of binder free electrodes in 6 M KOH electrolyte in three-electrode cell configuration. Fig. 8a shows the CV curves of three samples at a scanning rate of 5 mV/s. It is clearly seen that the CV curves of all three samples show quasi-rectangular shape. It is well known that the specific capacitance is proportional to the integral area of the CV curve at the same scanning rate. Therefore, PVA/Coal = 1/1 has higher capacitance than others. Fig. 8b shows the galvanostatic charge-discharge curves of three samples in the potential range from -1.1 V to -0.1 V at the specific current of 1 A g^{-1}. The curves showed quasi-triangular shape, indicating a well-defined electron double layer capacitive mechanism for the energy storage. The specific capacitance of the electrode was calculated by Eq. (2):

$$C_s = \frac{I\Delta t}{m\Delta V} \qquad (2)$$

Where I, Δt, m and ΔV are the applied current, discharge time, mass of the active material, and the potential window, respectively. According to Eq. (2), we can calculate the capacitance values at different specific currents from discharging time. The specific capacitances of samples were calculated according to Eq. (2). The results indicate that the PVA/Coal = 1/1 achieve the highest specific capacitance (170 F g^{-1}) at 1 A g^{-1} than PVA/Coal = 2/1 (133 F g^{-1}) and PVA/Coal = 1/2 (149 F g^{-1}). This may be due to the different mass ratio of PVA and coal produced different pore structure. Microporous structure and larger specific surface area can provide more electroactive sites for the adsorption of ions which contribute to the electron double layer capacitance, while the mesopores and channels in the fiber provided shorter diffusion route resulting in better performance at high current density. Therefore, the CPCFs (PVA/Coal = 1/1) with rich microporous and the larger mesoporous volume and total pore volume has the higher capacitance at each current densities (Fig. 8c). Fig. 8d,e present the CV plot of PVA/Coal = 1/1 fibers at various scanning rates and the galvanostatic charge-discharge curves at different current densities. Cycling stability is a key requirement for supercapacitors. The cycling stability of the PVA/Coal = 1/1 sample was investigated by repeating the charge/discharge test at current density of 2 A g^{-1} in 6 M KOH for 20,000 cycles (Fig.8f). The sample shows stable cycling performance and the specific capacitance increases about 5% after 20,000 cycles. The increase of the specific capacitance during the charge/discharge cycles is attributed to the activation process that allows the trapped ions to gradually diffuse out.[38]

Furthermore, the two-electrode cell was measured by assembling a symmetrical capacitor with 6 M KOH. Fig. S3a shows the CV curves of sample (PVA/Coal = 1/1) at a scanning rates from 5 to 100 mV/S, and the galvanostatic charge-discharge curves of it in the potential range from 0 V to 1 V at different current densities from 1 A/g to 50 A/g (Fig. S3b). The specific capacitance of a single electrode was calculated based on the following Eq. (3):

$$C_s = \frac{2I\Delta t}{m\Delta V} \qquad (3)$$

Where C_s is the specific capacitance of the electrode in farads per gram (F g^{-1}), I the discharge current in ampere (A), Δt the discharge time in seconds (s), m the mass of the single electrode in grams (g), and ΔV the voltage windows (0-1 V) in volts (V). We found that CPCFs (PVA/Coal = 1/1) exhibit specific capacitance of 79 F g^{-1} at 1 A g^{-1}. The normalized rate capability curves are given in Fig. S3c. The specific capacitance of the CPCFs decreases with increase in current density. For PVA/Coal = 1/1, the capacitance retention percentages at 50 A g^{-1} compared to it at 1 A g^{-1} is 58 %. The cycling performance of the two-electrode cell was evaluated by repeating charging and discharging for 1000 cycles at a current density of 1 A g^{-1} (Fig. S3d). The result shows that 68 % of the initial capacitance is retained for CPCFs.

Oil/water separation

The water contact angle of CPCFs was measured as shown in Fig.S4. It exhibited surface hydrophobicity, which water contact angle was 116.8°. Owing to their surface hydrophobicity, flexibility and mechanical stability, the CPCFs were highly efficient for separation/extraction of specific substances, such as organic pollutants and oils. When a small piece of flexible CPCFs was forced to the cottonseed oil, it

absorbed the oil completely in about ten seconds; After absorption, the fiber was direct combustion in air in order to remove the oil (Fig. 9a and Movie S1). The recyclability of the CPCFs is key criteria for oil/water separation. The absorption recyclability of CPCFs for oil absorption was measured using direct combustion method (Fig. 9b). The absorption capacities decreased to 67% after the first cycle and kept steady in the followed tests. After six absorption/combustion cycles, 59.2% for its original absorption capacities was achieved for cottonseed oil. The decrease was due to the mass loss during combustion. However, the abundant pore structure of CPCFs still remained after absorption and combustion, thus making it recyclable for many times.

Dye removal

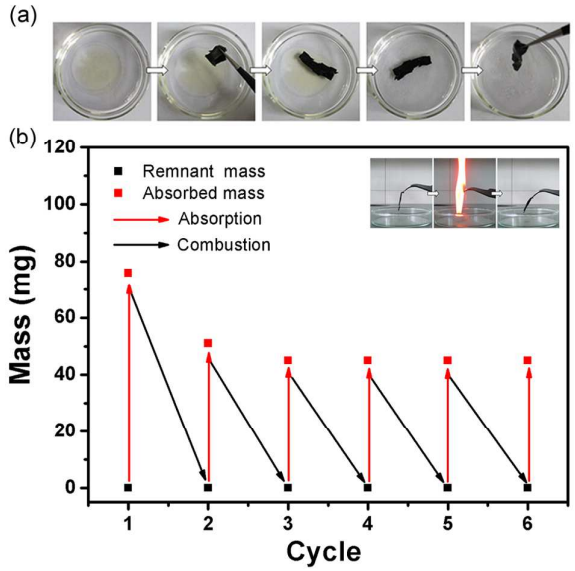

Fig. 9 (a) A layer of cottonseed oil was absorbed by a piece of CPCFs completely in 10 seconds. (b) Recyclability of CPCFs for absorption of cottonseed oil when using the direct combustion method. The insets show photographs of burning CPCFs saturated with cottonseed oil.

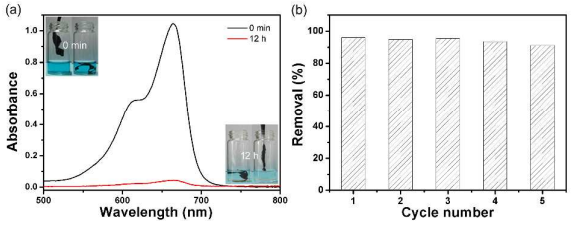

Fig. 10 (a) The UV-vis absorption spectra of the MB solution before and after the CPCFs kept 12 h. The insets show photographs of initial MB solution (20 mg/L) and treated with 1 mg CPCFs before and after 12 h. (b) The percentage removal of MB using the CPCFs in five cycles.

Based on large specific area and abundant porous structure of coal based carbon fibers, the removal of dye from model wastewater was assessed using CPCFs. Fig. 10a shows the UV-vis absorption spectra of the MB solution before and after adding fibers. The percentage of dye removal is beyond 95%. The insets show the photographs of initial MB solution (20 mg/L) and treated with 1 mg CPCFs before and after 12 h. The percentage removal of MB using it in five cycles was shown in Fig. 10b. We found it has good circulation for remove dyes from model wastewater. Therefore, the CPCFs is a proper alternative to remove dyes from colored aqueous solutions.

Conclusions

The coal can be dissolved in alkaline solution through the treatment by the mixture of concentrated sulfuric acid and nitric acid. Coal-based carbon porous nanofiber mats was then prepared via the electrospinning of two immiscible aqueous solutions (PVA and acid treated coal) followed by thermal treatment in an inert atmosphere. The porosity of the CPCFs can be controlled by varying PVA/Coal mass ratios in the precursor dispersion. Depending on the pore structures, the carbon fibers can be used as binder free supercapacitor electrodes and featured excellent electrochemical performances, which showed a capacitance of 170 F g^{-1} at the current density of 1 A g^{-1} in 6 M aqueous KOH electrolyte, and kept stably after 20,000 charge/discharge cycles at the current density of 2 A g^{-1}. Besides, the CPCFs was superhydrophobic, and showed outstanding performance in oil-absorption and good circulation for remove dyes from water. The coal-based porous carbon fibers represent an alternative promising candidate for wide range of energy storage and enviromental protection.

Acknowledgements

This work was supported by the National Natural Science Foundation of China (21262038 and U1203292), Specialized Research Fund for the Doctoral Program of Higher Education (2011650113001), the Outstanding Youth Natural Science Foundation of Xinjiang Uygur Autonomous Region of China (201311006), Scientific Research Program of the Higher Education Institution of Xinjiang (XJEDU2012I04).

Notes and references

1 S. H. Joo, S. J. Choi, I. Oh, J. Kwak, Z. Liu, O. Terasaki and R. Ryoo, *Nature*, 2001, **412**, 169.
2 M. D. Stoller, S. J. Park, Y. W. Zhu, J. An and R. S. Ruoff, *Nano Lett.*, 2008, **8**, 3498.
3 M. Inagaki, J. S. Qiu and Q. G. Guo, *Carbon*, 2015, **87**, 128.
4 S. Dutta, A. Bhaumik and K. C. W. Wu, *Energy Environ. Sci.*, 2014, **7**, 3574.
5 R. S. Haszeldine, *Science*, 2009, **325**, 1647.
6 M. Baikousi, C. Daikopoulos, Y. Georgiou, A. Bourlinos, R. Zbořil, Y. Deligiannakis and M. A. Karakassides, *J. Phys. Chem. C*, 2013, **117**, 16961.

7 Y. Yu, L. Gu, C. B. Zhu, P. A. v. Aken and J. Maier, *J. Am. Chem. Soc.*, 2009, **131**, 15984.
8 L. L. Zhang and X. S. Zhao, *Chem. Soc. Rev.*, 2009, **38**, 2520.
9 D. Lozano-Castellcó, J. Alcañiz-Monge, M. A. d. l. Casa-Lillo, D. Cazorla-Amorós and A. Linares-Solano, *Fuel*, 2002, **81**, 1777.
10 H. J. Lee, S. Choi and M. Oh, *Chem. Commun.,* 2014, **50**, 4492.
11 M. Gurrath, T. Kuretzky, H. P. Boehm, L. B. Okhlopkova, A. S. Lisitsyn and V. A. Likholobov, *Carbon,* 2000, **38**, 1241.
12 J. L. Figueiredo, *J. Mater. Chem. A,* 2013, **1**, 9351.
13 M. Sevilla and R. Mokaya, *Energy Environ. Sci.,* 2014, **7**, 1250.
14 W. Li, F. Zhang, Y. Q. Dou, Z. X. Wu, H. J. Liu, X. F. Qian, D. Gu, Y. Y. Xia, B. Tu and D. Y. Zhao, *Adv. Energy Mater.*, 2011, **1**, 382.
15 S. Nardecchia, D. Carriazo, M. L. Ferrer, M. C. Gutierrez and F. del Monte, *Chem. Soc. Rev.,* 2013, **42**, 794.
16 M. Ge, Z. M. Shen, W. D. Chi and H. Liu, *Carbon,* 2007, **45**, 141.
17 N. Saito, K. Aoki, Y. Usui, M. Shimizu, K. Hara, N. Narita, N. Ogihara, K. Nakamura, N. Ishigaki, H. Kato, H. Haniu, S. Taruta, Y. A. Kim and M. Endo, *Chem. Soc. Rev.,* 2011, **40**, 3824.
18 H. Hou and D. H. Reneker, *Adv. Mater.,* 2004, **16**, 69.
19 L. Y. Zhang, Y. Y. Wang, B. Peng, W. T. Yu, H. Y. Wang, T. Wang, B. W. Deng, L. Y. Chai, K. Zhang and J. X. Wang, *Green Chem.,* 2014, **16**, 3926.
20 M. Inagaki, Y. Yang and F. Y. Kang, Adv. Mater., 2012, **24**, 2547.
21 Y. H. Wang, J. R. Zeng, J. Li, X. Q. Cui, A. M. Al-Enizi, L. J. Zhang and G. F. Zheng, *J. Mater. Chem. A,* 2015, **3**, 16382.
22 J. Zeng, Q. Cao, X. Y. Wang, B. Jing, X. X. Peng and X. L. Tang, *J. Solid State Electrochem.,* 2015, **19**, 1591.
23 Y. X. Wang, X. F. Wen, J. Chen and S. N. Wang, *J. Power Sources,* 2015, **281**, 285.
24 A. V. Bazilevsky, A. L. Yarin and C. M. Megaridis, *Langmuir,* 2007, **23**, 2311.
25 H. Q. Wang, C. F. Zhang, Z. X. Chen, H. K. Liu and Z. P. Guo, *Carbon,* 2015, **81**, 782.
26 J. S. Im, J.-S. Jang and Y.-S. Lee, *J. Ind. Eng. Chem.,* 2009, **15**, 914.
27 D. Li and Y. N. Xia, *Nano Lett.,* 2004, **4**, 933.
28 C. Kim, Y. I. Jeong, B. T. N. Ngoc, K. S. Yang, M. Kojima, Y. A. Kim, M. Endo and J.-W. Lee, *Small,* 2007, **3**, 91.
29 S. X. Hu and Y.-L. Hsieh, *J. Mater. Chem. A,* 2013, **1**, 11279.
30 S. K. Lim, K. M. Cho, S. Tasaka and N. Inagaki, *Macromol. Mater. Eng.,* 2001, **286**, 187.
31 J. C. Wang and S. Kaskel, *J. Mater. Chem.,* 2012, **22**, 23710.
32 P. Chingombe, B. Saha and R. J. Wakeman, *Carbon,* 2005, **43**, 3132.
33 J. S. Qiu, Y. F. Li, Y. P. Wang, T. H. Wang, Z. B. Zhao, Y. Zhou, F. Li and H. M. Cheng, *Carbon,* 2003, **41**, 2170.
34 R. Q. Ye, C. S. Xiang, J. Lin, Z. W. Peng, K. W. Huang, Z. Yan, N. P. Cook, E. L. G. Samuel, C.-C. Hwang, G. Ruan, G. Ceriotti, A.-R. O. Raji, A. A. Marti and J. M. Tour, *Nat. Commun.,* 2013, **4**, 2943.
35 H. Y. Zhao, L. X. Wang, D. Z. Jia, W. Xia, J. Li and Z. P. Guo, *J. Mater. Chem. A,* 2014, **2**, 9338.
36 Y. Q. Dong, J. P. Lin, Y. M. Chen, F. F. Fu, Y. W. Chi and G. N. Chen, *Nanoscale,* 2014, **6**, 7410.
37 J. P. Mathews and A. L. Chaffee, *Fuel,* 2012, **96**, 1.
38 P. Simon and Y. Gogotsi, *Nat. Mater.,* 2008, **7**, 845.

Graphical Abstract

CPCFs with tunable internal channel was prepared via single-nozzle electrospinning, which exhibited excellent performance for energy storage and environmental protection.